Original Article

In vitro osteoinductive potential of porous monetite for bone tissue engineering

Journal of Tissue Engineering
Volume 5: 1–14

DOI: 10.1177/2041731414536572
tej.sagepub.com
SAGE

Bernadine Idowu, Giuseppe Cama, Sanjukta Deb and Lucy Di Silvio

Abstract

Tissue engineering–based bone grafts are emerging as a viable alternative treatment modality to repair and regenerate tissues damaged as a result of disease or injury. The choice of the biomaterial component is a critical determinant of the success of the graft or scaffold; essentially, it must induce and allow native tissue integration, and most importantly mimic the hierarchical structure of the native bone. Calcium phosphate bioceramics are widely used in orthopaedics and dentistry applications due to their similarity to bone mineral and their ability to induce a favourable biological response. One such material is monetite, which is biocompatible, osteoconductive and has the ability to be resorbed under physiological conditions. The osteoinductive properties of monetite in vivo are known; however, little is known of the direct effect on osteoinduction of human mesenchymal stem cells in vitro. In this study, we evaluated the potential of monetite to induce and sustain human mesenchymal stem cells towards osteogenic differentiation. Human mesenchymal stem cells were seeded on the monetite scaffold in the absence of differentiating factors for up to 28 days. The gene expression profile of bone-specific markers in cells on monetite scaffold was compared to the control material hydroxyapatite. At day 14, we observed a marked increase in alkaline phosphatase, osteocalcin and osteonectin expressions. This study provides evidence of a suitable material that has potential properties to be used as a tissue engineering scaffold.

Keywords

Mesenchymal stem cells, monetite, osteoinduction

Received: 7 February 2014; accepted: 19 April 2014

Introduction

Bone grafts are routinely used for the restoration of damaged bone. Ideally, natural bone grafts are the preferred choice, as they contain osteoprogenitor cells and osteoinductive growth factors and have osteoconductive properties. In the case of larger defects, however, synthetic biomaterials are now being used. More recently, interest has turned to cellular scaffolds, whereby the biomaterial provides a template and cues for cell differentiation and subsequent production of mineralized matrix. The success of tissue engineering relies on the ability to generate viable three-dimensional (3D) cell-seeded structures that have the same structural and functional capabilities as the host tissue. For bone regeneration, tissue-specific cells can be grown on scaffolds with appropriate properties to restore tissue function. The scaffold should closely mimic the native tissue and create an environmental niche that is able to elicit physiological responses and functionality similar to that of the native tissue.[1–3] The chemical composition and structure of the scaffold can act as a cue to recruit cells, allow cell adhesion, promote proliferation and differentiation.[4,5] The interaction of cells with scaffolds is fundamental in any regenerative medicine strategy. The success of a biomaterial regenerating bone is dependent on the outcome of a number of complex processes of which a rapid vascularization of the scaffold is of prime importance. Following implantation of a biomaterial with cells,

Biomaterials, Biomimetics & Biophotonics, Dental Institute, Guy's Hospital, King's College London, London, UK

Corresponding author:
Lucy Di Silvio, Biomaterials, Biomimetics & Biophotonics, Dental Institute, Guy's Hospital, King's College London, London, SE1 9RT, UK.
Email: lucy.di_silvio@kcl.ac.uk

interstitial fluid diffusion is the only source of nourishment for the cells on the biomaterial, and this is limited to a depth of about 200 μm into the biomaterial.[6,7] Furthermore, biological responsiveness is directly influenced by the material properties such as biocompatibility and surface chemistry influencing specific cells and their metabolic activities. Mesenchymal stem cells (MSCs) derived from human tissues have provided good prospects for cell-based tissue regeneration; they are readily available and an abundant source of cells. MSCs are multipotent, capable of self-renewal and have the potential to differentiate into chondrocytes, osteoblasts, adipocytes, fibroblasts, marrow stroma and other tissue of mesenchymal origin.[8] These human mesenchymal stem cells (hMSCs) reside in a diverse host of tissues throughout the adult organism and possess the ability to regenerate cell types specific for these tissues such as adipose tissue,[9] periosteum,[10] muscle,[11] synovial membrane[12] and human pulp tissue.[13]

Most calcium phosphate ceramics (CPCs) are osteoconductive by virtue of their surface characteristics that support cell adhesion and proliferation, while selected types exhibit osteoinductivity.[14] Calcium phosphates differ in their osteoconductive and osteoinductive properties, which are mainly attributed to the resorptive capacity and solubility of the different phases. However, the ability of selected calcium phosphates to exhibit intrinsic osteoinductive properties without the addition of osteogenic factors is not yet clearly understood. It is believed that either structural features are responsible for the in vivo osteoinductivity via the specific entrapment of bone morphogenetic proteins (BMPs) or it is due to the chemical composition of the material.[14,15] In addition, the type of calcium phosphate is also known to influence the potential osteoinductivity with biphasic calcium phosphate and tricalcium phosphates (TCP) being favoured over hydroxyapatite (HA).[16] It is thus natural to consider calcium phosphates as scaffolds for bone tissue engineering, given the similarity with the mineral composition of bone, biocompatibility and osteoconductive properties.[17] More recently, calcium phosphate cements such as brushite and monetite have been reported to be used as bone substitutes that can be formed in situ. Both exhibit the ability to be resorbed under physiological conditions albeit with different solubility at physiological pH, which are well tolerated in vivo. Monetite and brushite implants fabricated by 3D printing designed with open and closed porosity have also been reported to exhibit osteoinductive properties in vivo;[15] however, it is not apparent if the monetite itself is osteoinductive or the architecture of the scaffold led to in vivo bone formation. The potential of monetite as a bone substitute material is known, and with recent methodologies for easy conversion of brushite to monetite, it is now possible to fabricate custom-made shapes and sizes of monetite cements.[17,18] Monetite scaffolds have been reported to demonstrate suitable biocompatibility via in vitro cell culture and in vivo studies for hard tissue regeneration with a slower degradation profile than brushite as demonstrated in animal studies.[17,19,20] Monetite, however, has not yet been specifically explored as a scaffold for bone tissue engineering.

Thus, in this article, we report an in vitro study that aims to examine the osteoinductive potential of monetite as a scaffold, using hMSC in the absence of non-osteogenic supplements to assess the potential of its use as a 3D scaffold for bone tissue engineering.

Materials and methods

Scaffold fabrication

Discs of porous brushite scaffolds, d = 8.5 mm and h = 3.5 mm, were produced by manual mixing of equimolar quantities of β-TCP: $Ca_3(PO_4)_2$, assay ≥96% (Fluka, Germany), and monocalcium phosphate monohydrate (MCPM, $Ca(H_2PO_4)_2{\cdot}H_2O$), assay min. 98% (Sharlau, Spain) with sodium citrate solution as the liquid phase. And 60% by weight of sugar crystals with respect to the total calcium phosphate powder was used as the porogen. The brushite scaffolds were allowed to set for 24 h before removal of the porogen via dissolution in distilled water.[21] The macroporous brushite samples were converted to monetite by hydrothermal conversion using an autoclave at 121°C, 100% humidity for 30 min. Fourier transform–infrared/attenuated total reflection (FT-IR/ATR) spectra were obtained for the scaffolds using a PerkinElmer Spectrum One FT-IR Spectrometer (PerkinElmer, USA). X-ray diffraction (XRD) on the powder samples were carried out on a Bruker D8 Advance diffractometer equipped with a LYNXEYE detector, in flat plate geometry using Ni-filtered Cu-kα radiation. Data were collected in the range 2θ = 10°–100° with a step size of 0.02° and a count time of 12 s. The porous monetite cement blocks were scanned using micro–computed tomography (micro-CT) (Locus SP, micro-CT scanner; GE Healthcare, USA) set at a resolution of 7 μm.

Medium pore HA scaffolds, d = 8.5 mm and h = 3.5 mm (HA 0621), a gift from DyTech (UK) was used as a material control throughout the study. Scanning electron microscopy (SEM) was performed using a Hitachi S-3500 machine, and the sample microstructure recorded.

hMSC seeding density culturing conditions

Monetite scaffolds were washed overnight in phosphate-buffered saline (PBS) and left in culture medium 24 h prior to use to ensure complete removal of the porogen (sugar). This treatment did not lead to any changes in the monetitic phase, other than small traces of β-TCP as indicated by XRD (Figure 3). hMSCs were purchased from Lonza (Germany) and expanded to seed cells for 48 scaffolds at a

seeding density of 5×10^5 per scaffold. The cells were used at a maximum passage of 6. These were micro-seeded in 50 μL of medium onto the monetite scaffolds and HA scaffold in a 24-well plate which were allowed to adhere for 30 min, prior to flooding with non-osteogenic-conditioned medium containing high-glucose Dulbecco's modified Eagle's medium (DMEM) (D6429; Sigma–Aldrich, UK) supplemented with 20% foetal calf serum (FCS) (F9665; Sigma–Aldrich), 5 mL penicillin (100 U/mL) and streptomycin (0.1 mg/mL) (P0781; Sigma–Aldrich) as well as 10 ng human fibroblast growth factor (FGF) basic (Protech Inc, UK). They were left for 24 h and were further cultured in either non-osteogenic- or osteogenic-conditioned media, which were supplemented with 50 μm ascorbic acid, 10 nm dexamethasone and 10 mM β-glycerophosphate. The scaffolds were cultured for a period of 1, 14 and 28 days, with media change every 3 days. Monolayer cultures were set up in non-osteogenic media and treated accordingly. Cell lysates were collected for biochemical analysis and RNA for gene expression studies for all time periods. At day 14, both HA and monetite scaffolds seeded with hMSCs in non-osteogenic-conditioned media were fixed for immunofluorescent cytoskeletal staining. At day 42, the cell-seeded scaffolds in non-osteogenic-conditioned media were fixed to determine the level of collagen production.

Quantitative real-time reverse transcription–polymerase chain reaction (qPCR)

Extraction of RNA. At specific time periods, the media were removed from the well and replaced with 1 mL TRIzol (Ambion® AM9738). This was pipetted onto the scaffold and left for 24 h at −80°C. The TRIzol on the scaffold was then thawed and pipetted into a 2-mL, phase-lock, heavy gel tube (S Prime 2302830), and 200 μL of chloroform (C2432; Sigma–Aldrich) was added. This was shaken vigorously for 15 s and left for 1 min before spinning at 12,000 r/min in a bench top refrigerator for 15 min at 4°C. The aqueous phase containing RNA was removed and precipitated using 500 μl of Propan-2-ol (I9516; Sigma–Aldrich). This was placed at −80°C for 2 h or overnight to maximize the yield of RNA before being spun at 12,000 r/min for 20 min at 4°C to give a pellet. The supernatant was removed, and the pellet was washed using 75% ethanol. Ethanol was removed allowing the pellet to dry at room temperature for between 5 and 10 min. Depending on the size of the pellet, it was resuspended in 50 μL water or less and stored at −80°C until use.

Two-step reverse transcription–polymerase chain reaction method. Of the extracted RNA, 500 ng was used to conduct the first step of the two-step reverse transcription–polymerase chain reaction (RT-PCR) method. The first step was to transcribe RNA into complementary DNA (cDNA) according to a standard protocol using Applied Biosystems (UK) High-Capacity cDNA kit. Cycling conditions included 10 min at 25°C and 60 min at 37°C.

Real-time PCR. The second step was to PCR amplify the cDNA using the 7300 Real-Time PCR system (Applied Biosystems). A measure of 4 ng of cDNA was used per reaction, with the addition of 1 μL of the selected 20X TaqMan Gene Expression Assay Mix for each gene, namely, alkaline phosphatase (ALP), type IA collagen, osteocalcin (OCN), osteonectin, runt-related transcription factor 2 (Runx2) (all primers probes were purchased from Applied Biosystems, see Table 1), 10 μL TaqMan Fast Universal PCR Master Mix (2X) and water, this was made up to a total volume of 20 μL per well of a 96-well plate. The housekeeping gene *GAPDH* was used as endogenous standard as it was found to have the most consistent expression level, when compared to β-actin (data not shown). The expression for the gene of interest was normalized to *GAPDH* expression. Relative expression for each target gene was calculated using the $2^{-\Delta\Delta CT}$ method. The C_t values of each target gene were normalized by the C_t of the TaqMan human housekeeping gene *GAPDH* to obtain the ΔCT values. These values were subtracted by the C_t value of the calibrator which in this article is the hMSCs seeded on monetite and cultured in the presence of conditioned medium to obtain the ΔΔCT values.

This was performed in triplicates with the following cycler program: 95°C – 10 min and 40 cycles of 95°C – 15 s, 60°C – 1 min.

Semi-quantitative PCR analysis. PCR primers specific to human ALP 196-bp product (forward: 5′-CCACGTCTTCACATTTGGTG-3′; reverse: 5′-AGACTGCGCCTGGTAGTTGT-3′) and OCN 377-bp product (forward 5′-ATGAGAGCCCTCACACTCCT-3′; reverse 5′-CAAGGGGAAGAGGAAAGAAG-3′) were used in this study to amplify the cDNA, which was made previously.

A volume of 1 μL of cDNA was amplified using 12.5 μL GoTaq Green Master Mix 2X (Promega M7118) and 9.5 μL nuclease-free water (Promega P119A) per sample, and 10 pmol (1 μL each) of the forward and reverse primer was used, to give a final volume of 25 μL per reaction.

The following cycle was used: 96°C – 4 min, 35 cycles of 94°C – 30 s, 60°C – 45 s and 72°C – 59 s and finally 72°C – 10 min. The samples were then run on a 1.2% agarose gel which was stained using GelRed (Biotum GelRed™ 41003) to visualize the bands.

Biochemical analysis

DNA fluorimetric assay. The DNA fluorimetric assay in 96-well tissue culture plates using Hoechst 33258 was employed for this study to analyse the proliferative activity

Table 1. Osteogenic probes used for TaqMan assay.

Gene symbol	Gene name	Sequence	TaqMan assay ID
Runx2	Runt-related transcription factor 2	NM_001015051	Hs00231692_m1
ALP	Alkaline phosphatase	NM_001632.3	Hs03046558_s1
Col1A1	Type IA collagen	NM_000088.3	Hs00164004_m1
BGLAP	Osteocalcin (bone gamma-carboxyglutamate (gla) protein)	NM_199173.3	Hs01587814_g1
SPARC	Osteonectin (secreted protein acidic and rich in cysteine)	NM_003118.2	Hs00234160_m1

of HA and monetite scaffolds seeded with hMSCs in non-osteogenic media, where n = minimum of 3. Lysates were made using the standard freeze–thaw method of three cycles of freezing–thawing at 20-min intervals at −80°C and 37°C, respectively. It was conducted at days 1, 14 and 28, respectively. The optical absorbance values were obtained and represented graphically.

ALP activity using a microplate method. The ALP activity was measured using a microplate method described by Tsiridis et al.[22] to determine the alkaline activity of HA and monetite scaffolds seeded with hMSCs in non-osteogenic media. ALP activity was measured at 1, 14 and 28 days, using the lysates as described in the previous section.

OCN activity. A MicroVue competitive immunoassay (Quidel, USA) was used to determine the OCN levels for osteogenic differentiation, within HA and monetite scaffolds seeded with hMSCs in non-osteogenic media. These were examined from each group at 1, 14 and 28 days using the lysates as described in the previous section.

Cell morphology

Direct and indirect immunofluorescence of cytoskeletal elements. hMSCs were micro-seeded onto the monetite and HA scaffolds as mentioned previously and were allowed to expand for 2 weeks before being fixed with 4% paraformaldehyde containing 2% sucrose. This was fixed overnight at 4°C, before being washed with PBS. After rinsing, the cells were permeabilized at 4°C with 0.1% Triton X-100 for 15 min and further incubated with 1% bovine serum albumin (BSA) at 37°C for 10 min to prevent non-specific staining. This was followed by incubation with the appropriate primary and secondary antibodies at 37°C for 1 h. The washing buffer used was PBS + 0.5% Tween 20.

Direct cytoskeletal analysis using immunofluorescent labelling. Actin microfilaments were visualized using the direct stain phalloidin (1:100) (Sigma–Aldrich), this was incubated at 37°C for 1 h, washed in washing buffer and the nuclei was counterstained with 4′,6-diamidino-2-phenylindole (DAPI) for 5 min. Cells were then visualized under confocal microscope.

Indirect cytoskeletal analysis using immunofluorescent labelling. The cytoskeletal and adhesion proteins vimentin intermediate filaments (VIF) and vinculin (Sigma–Aldrich), respectively, were visualized using an indirect method. The primary antibodies used were monoclonal anti vimentin clone v9 (1:100) and monoclonal anti-vinculin (1:100). All antibodies were made up in 1% BSA + PBS and left for 1 h at 37°C; it was then washed several times using washing buffer and further incubated with the secondary antibody rabbit anti-mouse immunoglobulin G (IgG) fluorescein isothiocyanate (FITC) (1:50; Sigma–Aldrich) for an hour. Unbound secondary antibodies were washed off. The nuclei were counterstained with DAPI as described previously and visualized using confocal microscopy.

Type IA collagen matrix production using immunofluorescence labelling. Extracellular matrix protein type IA collagen staining was performed on the hMSC-seeded HA and monetite scaffolds cultured for 42 days. The primary antibody used was polyclonal rabbit anti-type IA antibody, and the secondary antibody was goat anti-rabbit IgG FITC (1:50; Sigma–Aldrich). The primary antibody was incubated for 1 h at 37°C, washed thoroughly with washing buffer and further incubated with secondary antibody. Unbound secondary antibodies were washed off. The nuclei were counterstained with DAPI and visualized using confocal microscopy.

Statistical analysis

All data were statistically analysed using an independent samples T-test at the 5% level employing the SPSS statistical package version 19 (IBM, USA).

Results

Scaffold fabrication

Porous brushite cements were converted to monetite using controlled hydrothermal conditions, by autoclaving at 121°C for 30 min yielding macroporous discs of monetite as shown in Figure 1. The XRD data recorded after the sample preparation showed the formation of brushite and monetite (Figures 2 and 3, respectively).

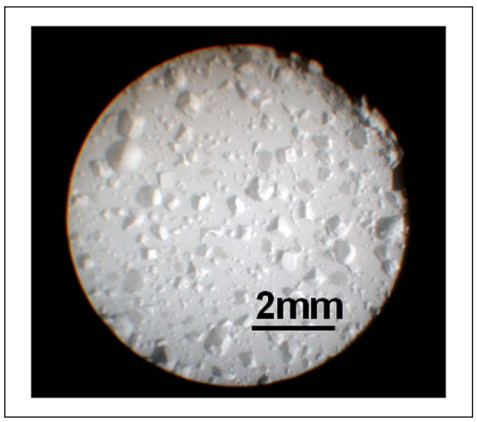

Figure 1. Optical image of monetite produced from brushite scaffold by autoclaving at 121°C for 30 min.

The two peaks appearing as a doublet at 3527, 3468, 3273 and 3171 cm^{-1} were due to νO–H vibration modes of the water in brushite. The formation of monetite was confirmed by FT-IR (Figure 4), which indicated the loss of the typical brushite peaks associated with the stretching frequencies (νOH: 3525–3153 cm^{-1}) and bend mode (δOH: 1645 cm^{-1}) due to the water crystallization present in the brushite crystal lattice (Figure 4). The micro-CT analyses conducted to determine porosity showed an average porosity of 45% and 70% for monetite and HA, respectively, with pore diameter between 200 and 650 μm.

Quantitative real-time reverse transcription-polymerase chain reaction (qPCR)

The gene expression of the early bone-specific marker *Runx2* (Figure 6(a)) examined over 28 days in test sample HA and monetite scaffolds seeded with hMSCs in non-osteogenic-conditioned medium showed that the monetite scaffold demonstrated an increasing trend that was not statistically significant over the 28-day time period while HA was reduced at day 14 but increased by day 28. Monolayer cell culture two-dimensional (2D) controls demonstrated an increase in Runx2 which decreased at day 28.

The gene expression of early bone-specific marker *ALP* quantified in monetite seeded with hMSCs in non-osteogenic-conditioned medium (see Figure 6(b)) demonstrated a significant increase in ALP activity on monetite and corresponds to cells following the normal cell cycle for differentiation.[23] The gene expression on the test control HA material was downregulated at all time periods. The amount of *ALP* expression in the monolayer cell culture 2D control demonstrated similar amounts to the HA control material.

The gene expression of late bone-specific marker *OCN* measured in test sample HA and monetite scaffolds seeded with hMSCs (Figure 6(c)) showed a reduction in the expression from days 1 to 14, but by day 28, there was a marginal increase within the two groups. The cells seeded on the monetite scaffold, however, showed a significant increase ($p < 0.05$) in *OCN* in comparison with HA control scaffold. Surprisingly, the *OCN* expression in the monolayer cell culture 2D controls showed statistically high expression in comparison with the test scaffolds examined at all time periods.

The gene expression of early bone-specific marker osteonectin quantified in monetite seeded with hMSC in non-osteogenic-conditioned media (Figure 6(d)) peaked at day 14, but by day 28, it was downregulated, which confirms osteogenic differentiation of hMSC. Osteonectin was observed to peak at 14 days in monetite, whereas on the test control, HA scaffold, this occurred much later at day 28. The level of osteonectin expression remained constant in the monolayer cell culture 2D control for all time points.

Type IA collagen exhibited a gradual increase in the monetite scaffold seeded with hMSCs over the 28-day time period, while the test sample HA scaffold seeded with hMSC after 14 days did not change (Figure 6(e)). The level of gene expression of type IA collagen at days 14 and 28 in cell-seeded monetite scaffold exceeded that of cell-seeded HA scaffold, while the level of collagen expression in monolayer cell culture 2D control remained the same over time.

ALP and *OCN*, early and late osteoblast-specific gene expression markers visualized using semi-quantitative RT-PCR over 28 days in both non-osteogenic- and osteogenic-conditioned media, show different band intensities with a greater intensity in the presence of osteogenic-conditioned media as was expected (Figure 6(f)).

Biochemical analysis

ALP/DNA assay. Figure 7(a) shows the proliferative (DNA) and differentiation potential (*ALP* early marker) of HA and monetite scaffolds seeded with hMSCs in non-osteogenic-conditioned medium, with the monetite scaffold demonstrating a statistically significant increase in ALP/DNA ($p < 0.001$) when compared with the material control HA at all time periods.

OCN production. On examining *OCN* using a competitive immunoassay at the protein level (Figure 7(b)), HA showed a statistically significant ($p < 0.01$) increase and production over time when compared to the hMSC-seeded monetite scaffold although monetite did show an increase with time.

Figure 8 shows a representative area of hMSC monolayer culture, from the same batch of cells which were seeded onto the monetite and HA scaffold. Staining of the cytoskeleton revealed the presence of an organized cytoplasmic morphology of the cells, with the presence of

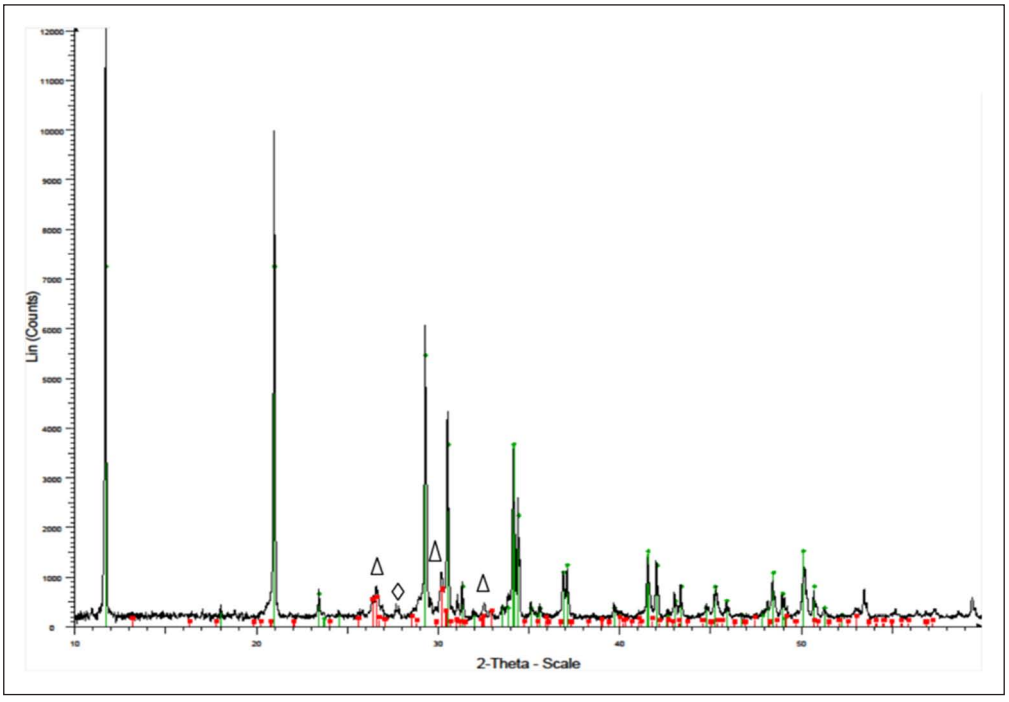

Figure 2. X-ray pattern of brushite cement.
The green line represents the main brushite peaks (JCPDS file 00-009-0077) and the red line represents the main (Δ) monetite peaks (JCPDS file 00-009-0080). (◊) Main β-tricalcium phosphate peaks (JCPDS file 00-009-0169).

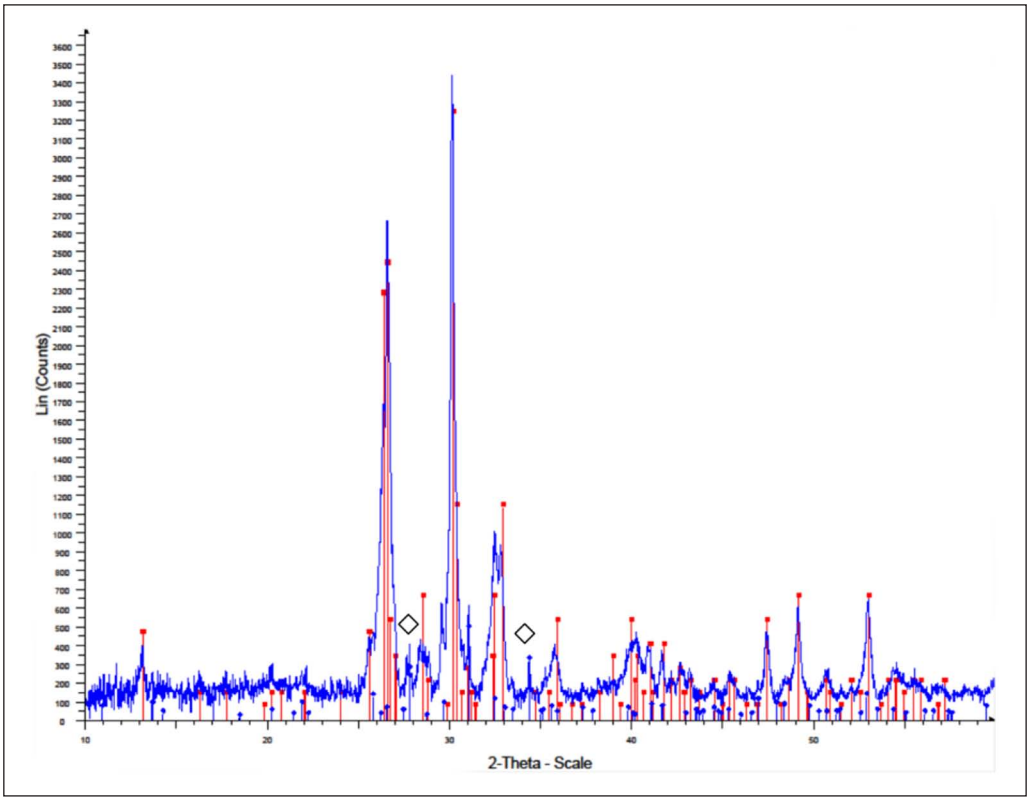

Figure 3. X-ray pattern of monetite scaffold.
The red line represents the main monetite peaks (JCPDS file 00-009-0080) and the blue line represents the main (◊) β-tricalcium phosphate peaks (JCPDS file 00-009-0169).

stress fibres stained using phalloidin, demonstrating fibroblast-like morphology of the hMSC.

Using direct and indirect immunofluorescent methods, the cytoskeletal protein actin microfilaments, intermediate filaments and the focal adhesion protein vinculin were used to demonstrate the cell morphology and organization at day 14 within the 3D fractured scaffold. The staining was cytoplasmic as expected. Figure 9(a), (c) and (e) showed the stain in the absence of nuclei and Figure 9(b), (d) and (f) shows images with the nuclei counterstained. No positive staining was observed within the control samples (data not shown).

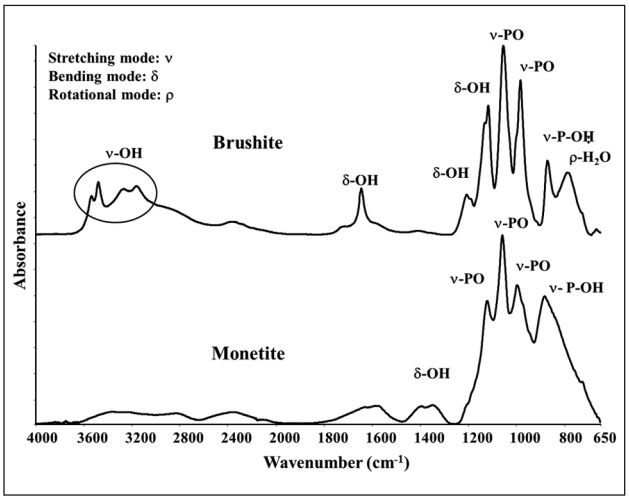

Figure 4. FT-IR spectra of the cements indicating the formation of brushite and monetite.
FT-IR: Fourier transform–infrared spectroscopy.

Figure 9(a) and (b) shows the stress fibres within the cell (arrows), Figure 9(c) and (d) demonstrates the visible cytoplasmic staining of the structural intermediate filaments showing the structural integrity of the cells (asterisks (*)). The cells demonstrate maintenance of their morphology as shown in Figure 8. While Figure 9(e) and (f) illustrates the focal adhesion as stained using indirect staining for vinculin present mainly in form of cytoplasmic and diffuse staining due to the cell–cell and cell–matrix interactions as clearly seen (arrow heads).

The level of type 1A collagen production, which is a measure of matrix deposition within the HA and monetite fractured scaffolds seeded with hMSC in non-osteogenic-conditioned media over 42 days, is illustrated in Figure 10. Type IA collagen staining was conducted. Figure 10(a) and (b) shows staining within HA scaffold (arrow heads), while Figure 10(c) and (d) shows staining within monetite scaffold (arrows). It was observed that the collagen production in the monetite scaffold was greater than that of the HA scaffold. The nuclei were counterstained to ensure differentiation between background staining and matrix staining as a result of collagen production. No staining was observed within the control sample (data not shown).

Discussion

Scaffolds for bone tissue engineering would be ideal if they exhibited inherent osteoinductive properties apart from biocompatibility, osteoconductivity and

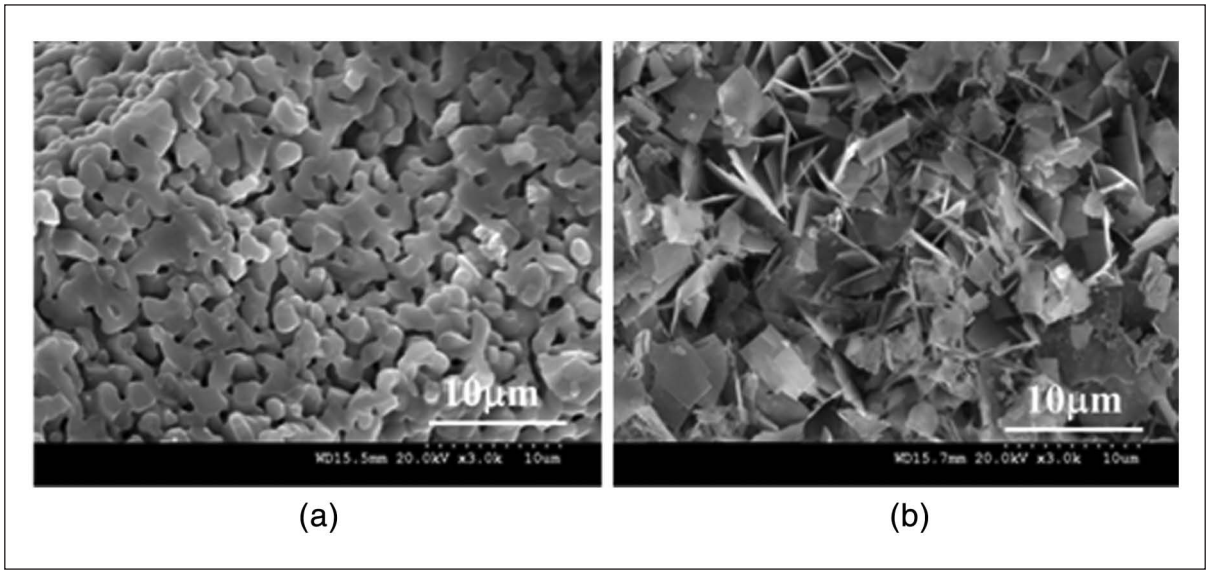

Figure 5. The microstructure of (a) HA sample shows rounded crystals and (b) monetite shows needle-like crystals typical of a monetite phase.
HA: hydroxyapatite.

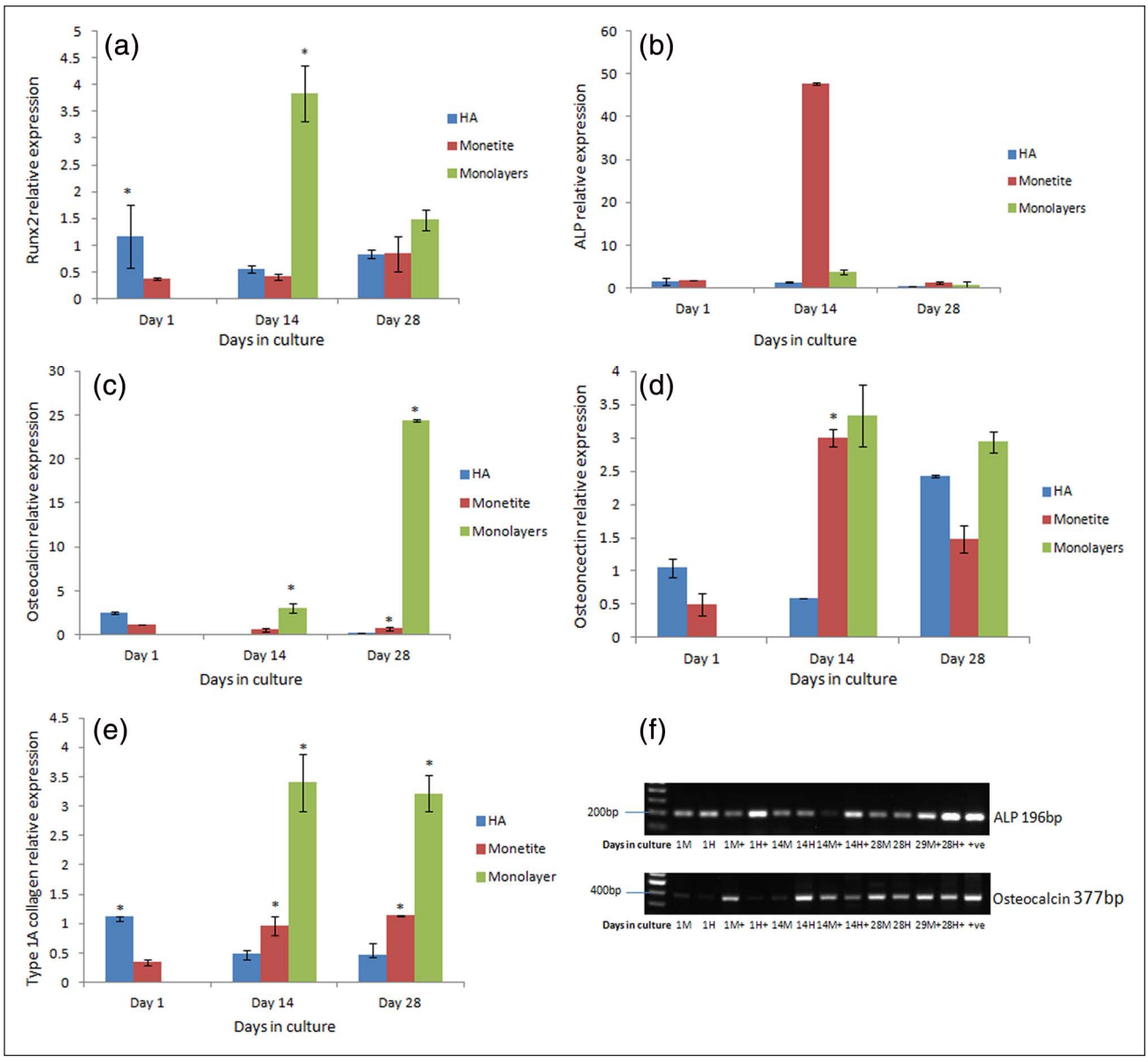

Figure 6. (a) *Runx2* gene expression over 28 days of monetite and HA scaffolds with monolayer cultures seeded with hMSC in non-osteogenic-conditioned medium ($p < 0.05$), (b) *ALP* gene expression over 28 days of monetite and HA scaffolds with monolayer cultures seeded with hMSC in non-osteogenic-conditioned medium ($p < 0.05$), (c) osteocalcin gene expression over 28 days of monetite and HA scaffolds with monolayer cultures seeded with hMSC in non-osteogenic-conditioned medium ($p < 0.05$), (d) osteonectin gene expression over 28 days of monetite and HA scaffolds with monolayer cultures seeded with hMSC in non-osteogenic-conditioned medium ($p < 0.05$), (e) type IA collagen gene expression over 28 days of monetite and HA scaffolds with monolayer cultures seeded with hMSC in non-osteogenic-conditioned medium ($p < 0.05$) and (f) semi-quantitative RT-PCR analysis of HA and monetite scaffolds seeded with hMSCs in non-osteogenic and osteogenic-conditioned medium (M = monetite in non-osteogenic medium, H = HA in non-osteogenic-conditioned medium, M+ = monetite in osteogenic-conditioned medium, H+ = HA in osteogenic-conditioned medium).
HA: hydroxyapatite; hMSCs: human mesenchymal stem cells; RT-PCR: reverse transcription–polymerase chain reaction.

degradability. Calcium phosphate–based materials such as HA, tricalcium phosphate (β-TCP), dicalcium phosphate dihydrate (brushite) and monetite (anhydrous form of brushite) are the most favoured resorbable materials for scaffolds and bone substitutes as they exhibit similarity to the mineral component of bone. However, the solubility and resorption rates of the calcium phosphates differ which governs their suitability as candidates for tissue engineering scaffolds. HA is the most stable form with an extremely slow rate of resorption, whereas brushite has been reported to resorb rapidly in vivo. On the other hand, monetite, the anhydrous form of brushite, initially exhibits a slower rate

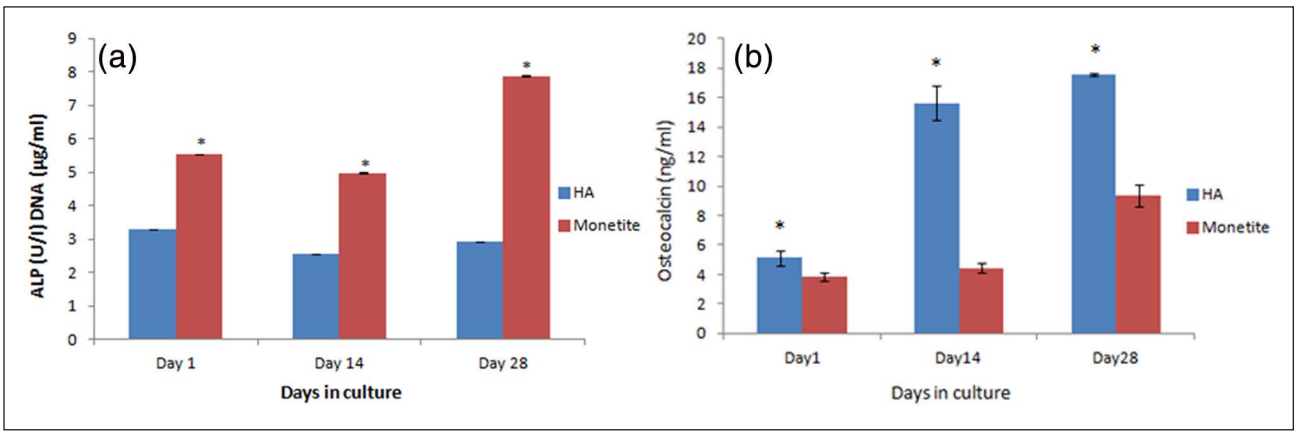

Figure 7. (a) ALP/DNA content of HA and monetite scaffolds seeded with hMSCs in non-osteogenic-conditioned medium 28 days ($p < 0.001$) and (b) osteocalcin production of hMSC seeded in HA and monetite in non-osteogenic-conditioned medium ($p < 0.01$).
HA: hydroxyapatite; hMSCs: human mesenchymal stem cells.

of resorption but does not transform to the HA phase,[17] thus potentially more suited as a scaffold for bone tissue engineering.

Macroporous monetite scaffolds were prepared by the hydrothermal conversion of brushite, and the porosity was obtained via the loss of sugar, the soluble porogen. The XRD and FT-IR patterns (Figures 2–4) confirmed the formation of monetite with porosity over 45%, which were seeded with human MSC (hMSC) in the absence of differentiating factors, with experiments being conducted under static conditions. Porous HA blocks were used as the material control, while monolayer cultures were used as a cell control. It should be noted, however, that only data for the monetite test scaffolds and the control HA are comparable as they are a 3D structure; the 2D monolayer serves as a cell control for environmental conditions and to monitor normal cell behaviour. Hence, 2D and 3D culture conditions will show differences in differentiation and gene expression, as observed in this study.

The standard conditions for osteogenic differentiation of stem cells in vitro are treatment with dexamethasone (known to induce *Runx2* expression by upregulation of *TAZ* and *MKP1*), ascorbic acid (increases type IA collagen secretion) and β-glycerophosphate (serves as a phosphate source for mineralization).[24] However, in order to confirm osteoinductivity, there should be evidence of the material recruiting undifferentiated osteoprogenitor cells that are not yet committed to the osteogenic lineage to form osteoprogenitor cells.[25] While there have been several reports in the literature where osteoinduction has been shown in vivo,[15,26,27] fewer have been reported in vitro. Tamimi et al.[17] examined the properties of both monetite and brushite scaffolds in vitro and in vivo using mouse bone marrow. Although the study of Tamimi demonstrated similar findings with cells cultured on monetite surfaces expressing messenger RNA (mRNA) characteristic of osteogenic genes, it is not directly comparable to this study, as their

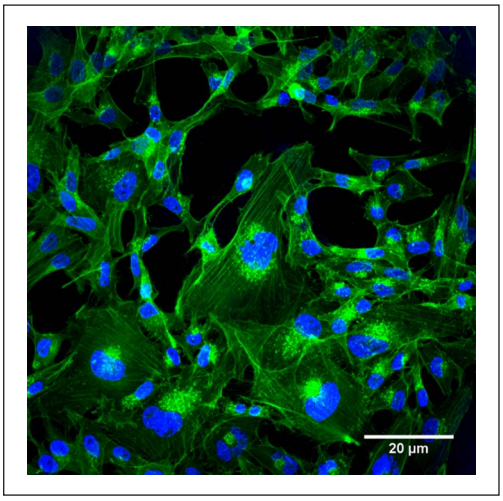

Figure 8. Confocal laser scanning microscopy (CLSM) – direct staining of actin microfilament cytoskeletal protein and nuclei counterstained with DAPI at day 3 of monolayer culture.
DAPI: 4′,6-diamidino-2-phenylindole.

experiment was conducted in the presence of exogenous soluble differentiating factors, while in this study this was not the case.

Parekh et al.,[28] Oh et al.[29] and Dalby et al.[30] have attempted to look at osteoinduction on nanoscale scaffolds in vitro using hMSCs differentiation into osteogenic lineages without any exogenous soluble differentiation: the overall consensus was that the predetermined micropattern and geometries of the scaffold play a role in the cell–scaffold interaction. Langer and Tirrell[31] and Hollister et al.[32] also confirmed the importance of the structural properties of the bone substitutes which should be accurately defined, since the surface morphology, stiffness or topography of the scaffolds can directly affect cell–scaffold interaction and hence the desired tissue formation. We show two SEM

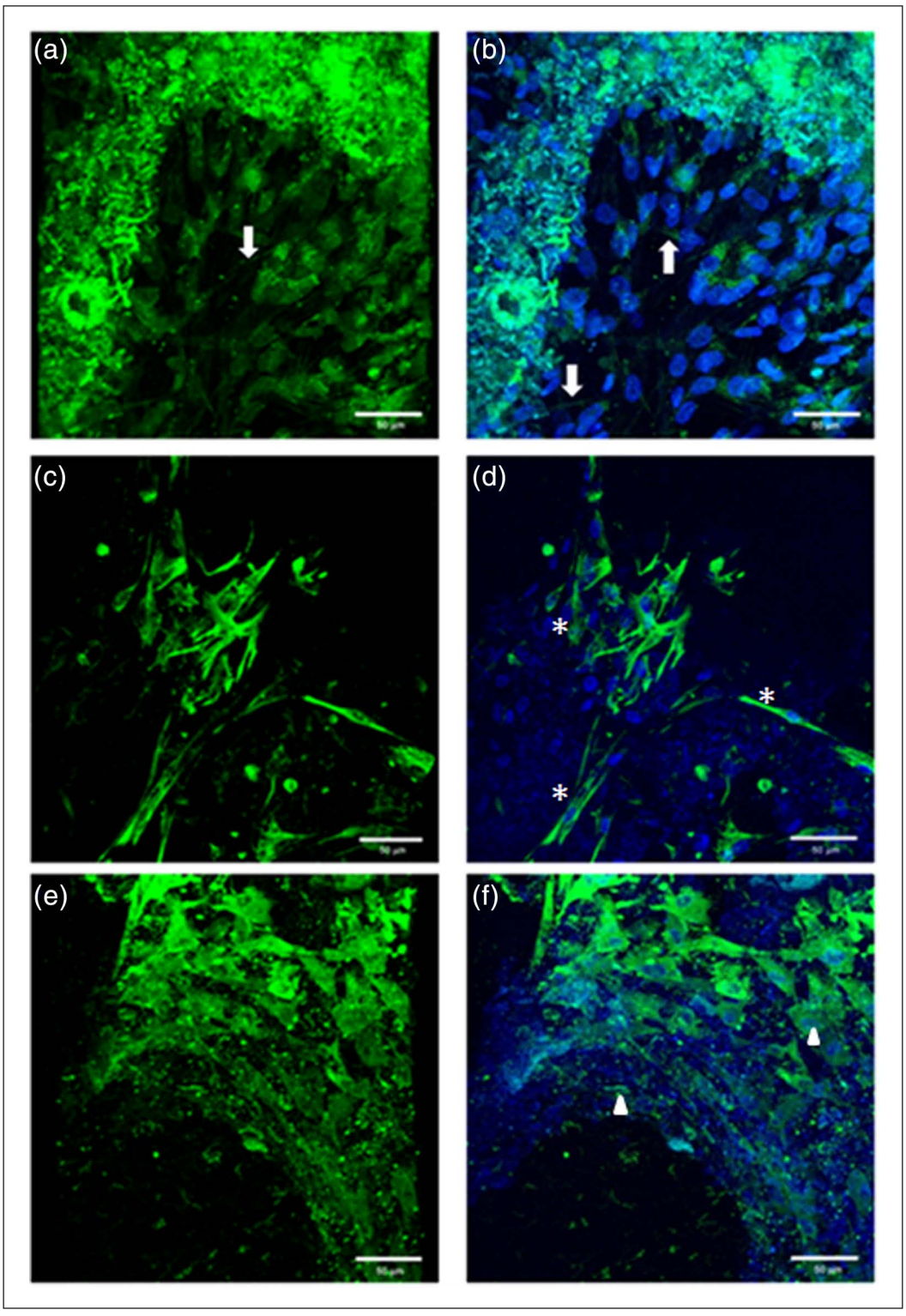

Figure 9. CLSM demonstrating the morphology of hMSCs seeded on monetite in non-osteogenic-conditioned media at day 14 (a, c, e) without nuclei staining and (b, d, f) with nuclei staining. (a, b) Direct staining for actin microfilament cytoskeletal proteins, arrows demonstrating the stress fibres for F-actin microfilaments; (c, d) indirect staining for intermediate filaments cytoskeletal protein, asterisks (*) denoting the fibroblast-like cell morphology; and (e, f) indirect staining for adhesion molecule vinculin, arrow heads showing the focal adhesion proteins either within the cell cytoplasm or staining on the scaffold.
CLSM: confocal laser scanning microscopy; hMSCs: human mesenchymal stem cells.

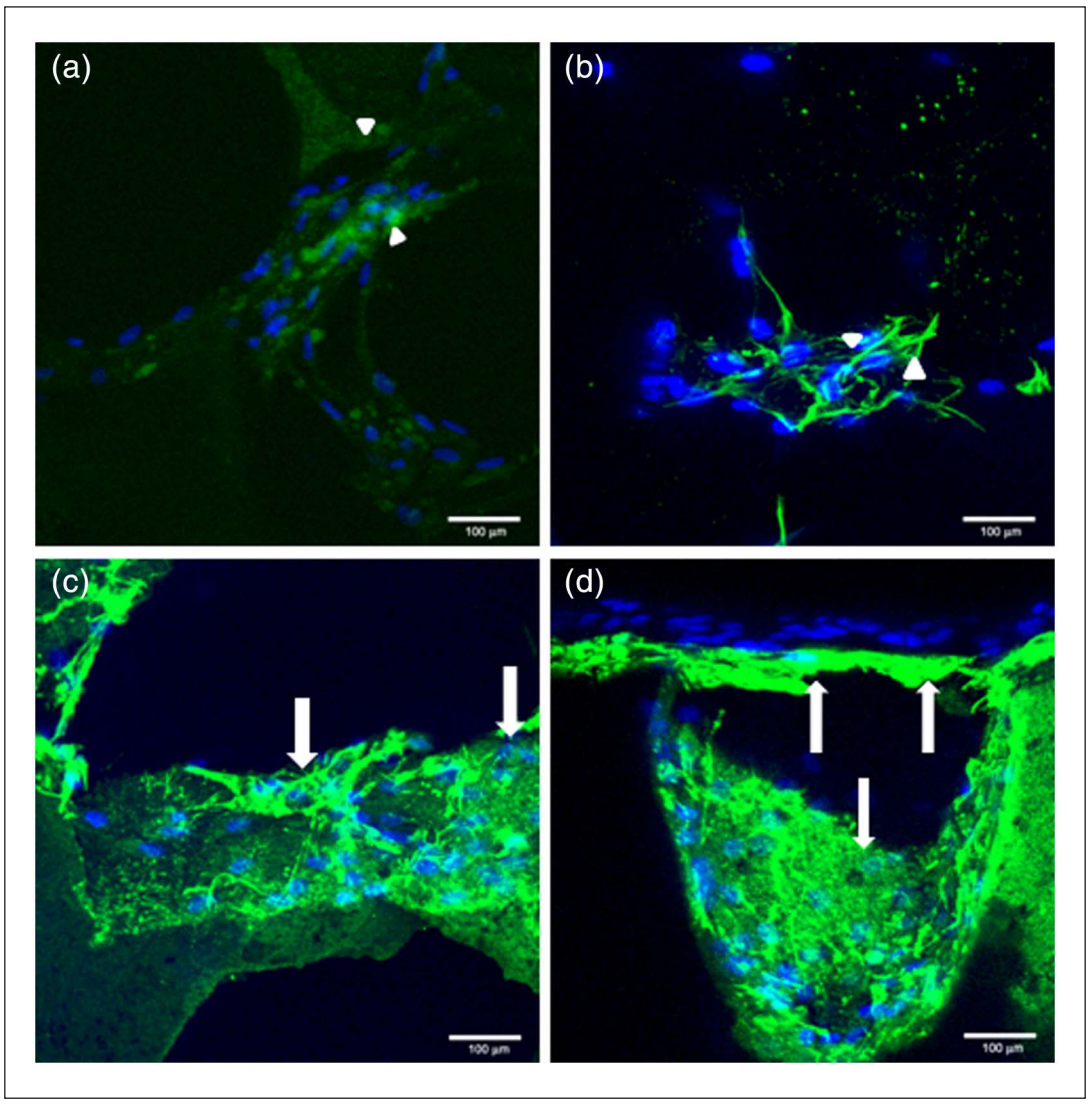

Figure 10. CLSM demonstrating collagen matrices deposited in non-osteogenic-conditioned medium at day 42 in hMSC seeded in HA and monetite scaffolds counterstained with nuclei (a, b) HA, arrow heads demonstrating low-level staining of type IA collagen, and (c, d) monetite scaffold, arrows demonstrating strong staining surrounding cell nuclei.
CLSM: confocal laser scanning microscopy; hMSCs: human mesenchymal stem cells; HA: hydroxyapatite.

images (Figure 5(a) and (b)), one for HA and the other for monetite scaffold; the difference in porosity and crystal structure does affect the cell–scaffold interaction as illustrated by our findings.

The *Runx2* osteogenic-specific transcription marker was upregulated in hMSCs when cultured on monetite scaffolds over the 28-day time period (Figure 6(a)). This upregulation may be attributed to the solubility of the porous scaffold and production of ionic species in comparison with the stable HA scaffold. *Runx2* has been described as the 'master gene' for osteoblast differentiation as it is required for the expression of OCN.[33] Usually after the osteoblast reaches maturity, *Runx2* expression should be reduced, but as shown in this study, up to 28 days *Runx2* is still being expressed (Figure 6(a)), hence confirming the osteoblasts have not fully matured. Maruyama et al.[34] showed evidence of this in their model. The data from this study have been confirmed by the low level of late bone-specific marker *OCN* at day 28 on monetite scaffold seeded with hMSCs (Figure 6(c)). It was further observed that the *Runx2* and *OCN* genes in HA scaffold seeded with hMSCs were also upregulated (Figures 6(c) and 7(b)), which suggests that HA may have some intrinsic osteoinductive properties; this has been described previously in the literature.[28,29,37]

Early markers of osteogenic differentiation, *ALP* and osteonectin (Figure 6(b) and (d)), peaked at day 14 in cells cultured on the monetite scaffold, which corresponds to the normal cell cycle in differentiation; however, interestingly, at the protein level, we see a gradual increase in *ALP*

over the 28-day time period. Temporal sequence of osteoblastic phenotypic genes defines the passage from proliferation, matrix development and mineralization. *ALP* is a key phosphate necessary for bone formation, and phosphatases are known to cleave phosphates from several matrix proteins. The cleaved phosphate is responsible for the formation of calcium phosphate crystals. The phosphorylated proteins present in the deposited extracellular matrix could trigger downstream signalling events leading to upregulation of *ALP* in deposited matrix on scaffolds,[36] which may explain the findings of high protein levels at day 28 (Figure 7(a)). Lian and Stein[23] have reported that immediately following the proliferative peak, there is a drop in DNA synthesis, and the expression of *ALP* increases between 10 and 14 days. The subsequent drop after day 14 is possibly reflective of the cells entering a matrix maturation phase and mineralization.

As described by Wang et al.,[37] osteonectin interacts with extracellular collagen matrix protein and cytokines contributing to the regulation of osteoblastic growth; in this study, a peak in osteonectin was observed at day 14 (Figure 6(d)), demonstrating its involvement in the differentiation of hMSCs seeded on monetite.

Type 1A collagen also a marker of osteogenic differentiation showed a gradual increase with time for cells cultured on monetite (Figure 6(e)), which was confirmed at the protein level through the immunofluorescent staining at day 42 as shown in Figure 10(c) and (d). For the material HA control scaffold, however, findings from the protein level correlated with the level of gene expression, which was a reduction of collagen expression over time (Figure 7(a) and (b)). Lian and Stein[23] described type IA collagen as being expressed initially and then being downregulated during subsequent bone cell maturation, which confirms the findings from previous discussions that the differentiated osteoblasts had not yet reached maturity.

The results from the molecular and protein analysis demonstrated the successful proliferative and differentiating properties of hMSCs and the maintenance of their osteogenic phenotype in non-osteogenic-conditioned media over 28 days in culture when seeded on the porous monetite discs. In agreement with other authors, there may not always be a correlation between gene expression and protein production.[38,39] The transcription-level data suggest that a specific protein is being expressed, but the lack of precise correlation stems from the fact that there are various processes involved in between transcription and translation. For example, the half life of protein and mRNA are very different, which could complicate the finding/correlation.

A porous HA was used as the material control, and the ALP/DNA ratio was observed to be much lower, which may be attributed to the differences in the overall porosity as also reported by Yamasaki and Sakai,[27] who showed HA has different properties including porosity, than other ceramics. This may favour some gene expression over others, for example, *Runx2* as seen in Figure 6(a). Wang et al.[37] and Tamimi et al.[17] studied at the mRNA level characteristics of osteoblasts and observed that the solubility products released from the bioceramics influenced the gene expression resulting in up- or downregulation of osteogenic genes. The gene expression levels demonstrated within the monetite scaffold in comparison with the HA suggests a function of the Ca:P ratio and the properties of the scaffold, in terms of the level of adsorption of the protein, the roughness of the scaffold and the level of porosity which is thought to enhance the ion exchange with culture medium and possibly act as a central point for the precipitation of dissolved calcium phosphates.

Porosity of the scaffold and hence lack of migration of the cells within the scaffold can affect the gene expression as also reported by Salim et al.[40] Clustering of the cells in areas may give rise to transient changes in oxygen and this may have some effect on osteogenic differentiation. Feng et al.[41] have alluded to the fact that some genes are sensitive to hypoxia, which is a consequence of cells that have not migrated through the scaffold and are concentrated around the surface. This, therefore, does not allow for diffusion of nutrients and oxygen as mentioned previously.

A representative image of hMSCs used, cultured as a monolayer (Figure 8) immunofluorescently stained for actin filaments, showed the typical phenotype of hMSC with a fibroblast-like morphology, such features remained visible as demonstrated in Figure 9(a) and (b) on the monetite scaffold. The cell spreading and the presence of VIFs (Figure 9(c) and (d)) are suggestive of possible mechanotransduction events taking place, with staining for focal adhesion protein vinculin (Figure 9(e) and (f)), demonstrating the ability of cells to adhere to the scaffolds. All these events, therefore, demonstrate normal cell–cell and cell–matrix interactions visible on the monetite scaffold. Such interactions facilitate signal transduction and hence influence the cell behavior.[42]

This in vitro study investigated the behaviour of hMSCs on monetite scaffold in non-conditioned media and demonstrated similar properties to the control HA and some 'potential intrinsic' osteoinductive characteristics. From literature findings, it is evident that osteoinductivity varies with the type and properties of the calcium phosphate. For example, Muller et al.[43] showed elevated expression of *OCN* and bone sialoprotein (BSP) mRNA by human bone marrow stromal cells (BMSCs) cultured on BONIT matrix, when compared to cells grown on tissue culture plastic. Polini et al.[44] showed that the same cell type in the absence of osteogenic supplements expressed higher levels of *Runx2* and *BSP* mRNA on polycaprolactone nanoparticles loaded with TCP particles compared to nanofibers loaded with HA particles. In contrast, Guha et al.[45] showed that BMSCs cultured on HA/TCP biphasic substrates produced more *OCN* than cells cultured on HA. We observed similar

findings when we compared the expression of *OCN* mRNA on monetite compared with HA (Figure 7(b)). These findings, therefore, suggest that calcium phosphates can significantly influence osteoinduction.

It is known that bioresorbability of sintered HA is very different to calcium phosphate cements such as brushite or monetite. Monetite is known to exhibit higher resorbability in aqueous solutions, the degradation rates thus differ, and the amounts of Ca^{2+} and phosphate (PO_4^{3-}) ions released are vastly different, which may be one of the reasons for the different observations noted between the two scaffolds.[14,46] Cellular response is indeed affected by the composition of calcium phosphate, and the release of calcium ions from scaffolds plays a major role in influencing osteoblastic differentiation, through the activation of specific pathways such as activation of the calmodulin-dependent protein kinase type II α/Crassulacean acid metabolism (CaMK2α/CAM) pathway, which may modulate differentiation via the cyclic adenosine monophosphate (cAMP) response element-binding protein (CREB) and/or the extracellular signal-related kinase 1/2 (ERK1/2) pathway.[16,47,48]

In conclusion, this study primarily focused on the ability of the scaffold to facilitate differentiation of hMSCs towards osteogenic differentiation in the absence of external additives, that is, non-osteogenic-conditioned medium. hMSCs retained their normal cellular physiology, morphology and proliferation, and the monetite scaffold demonstrated similar properties to the control HA and some 'potential intrinsic' osteoinductive characteristics. Although the exact mechanism is not clearly understood, the results indicate the viability and potential advantage of the use of monetite scaffolds, which warrants further investigation.

Declaration of conflicting interests

The authors declare that there is no conflict of interest.

Funding

This work was financially supported by the Centre of Excellence in Medical Engineering funded by the Wellcome Trust.

References

1. Bose S and Tarafder S. Calcium phosphate ceramic systems in growth factor and drug delivery for bone tissue engineering: a review. *Acta Biomater* 2012; 8: 1401–1421.
2. William DF. On the mechanisms of biocompatibility. *Biomaterials* 2008; 29: 2941–2953.
3. Olszta MJ, Cheng X, Jee S, et al. Bone structure and formation: a new perspective. *Mater Sci Eng R Rep* 2007; 58: 77–116.
4. Hubbell JA. Biomaterials in tissue engineering. *Nat Biotechnol* 1995; 13: 565–576.
5. Hollister SJ. Porous scaffold design for tissue engineering. *Nat Mater* 2005; 4: 518–524.
6. Aronson J. Temporal and spatial increases in blood flow during distraction osteogenesis. *Clin Orthop Relat Res* 1994; 301: 124–131.
7. Carmeliet P and Jain RK. Angiogenesis in cancer and other diseases. *Nature* 2000; 407: 249–257.
8. Pittenger MF, Mackay AM, Beck SC, et al. Multilineage potential of adult human mesenchymal stem cell. *Science* 1999; 284: 143–147.
9. Zuk PA, Zhu M, Mizuno H, et al. Multilineage cells from human adipose tissue: implications for cell-based therapies. *Tissue Eng* 2001; 4: 211–228.
10. Nakahara H, Goldberg WM and Caplan AI. Culture-expanded human periosteal-derived cells exhibit osteochondral potential in vivo. *J Orthop Res* 1991; 9: 465–476.
11. Bosch P, Musgrave DS, Lee YJ, et al. Osteoprogenitor cells within skeletal muscle. *J Orthop Res* 2000; 18: 933–944.
12. De Bari C, Dell'Accio F, Tylzanowski P, et al. Multipotent mesenchymal stem cells from adult human synovial membrane. *Arthritis Rheum* 2001; 44: 1928–1942.
13. Egbuniwe O, Idowu BD, Funes JM, et al. P16/p53 expression and telomerase activity in immortalized human dental pulp cells. *Cell Cycle* 2011; 22: 3912–3919.
14. LeGeros RZ. Calcium phosphate-based osteoinductive materials. *Chem Rev* 2008; 108: 4742–4753.
15. Habibovic P, Gbureck U, Doillon CJ, et al. Osteoconduction and osteoinduction of low-temperature 3D printed bioceramic implants. *Biomaterials* 2008; 29: 944–953.
16. Samavedi S, Whittington AR and Goldstein AS. Calcium phosphate ceramics in bone tissue engineering: a review of properties and their influence on cell behavior. *Acta Biomater* 2013; 9: 8037–8045.
17. Tamimi F, Le Nihouannen D, Eimar H, et al. The effect of autoclaving on the physical and biological properties of dicalcium phosphate dihydrate bioceramics: brushite vs. monetite. *Acta Biomater* 2012; 8: 3161–3169.
18. Cama G, Gharibi B, Sait MS, et al. A novel method of forming micro- and macroporous monetite cements. *J Mater Chem B* 2013; 1: 958–969.
19. Gbureck U, Hozel T, Klammert U, et al. Resorbable dicalcium phosphate bone substitutes prepared by 3D powder printing. *Adv Funct Mater* 2007; 17: 3940–3945.
20. Klammert U, Reuther T, Jahn C, et al. Cytocompatibility of brushite and monetite cell culture scaffolds made by three-dimensional powder printing. *Acta Biomater* 2009; 5: 727–734.
21. Cama G, Barberis F, Botter R, et al. Preparation and properties of macroporous brushite bone cements. *Acta Biomater* 2009; 5: 2161–2168.
22. Tsiridis E, Bhalla A, Ali Z, et al. Enhancing the osteoinductive properties of hydroxyapatite by the addition of human mesenchymal stem cells, and recombinant human osteogenic protein-1 (BMP-7) in vitro. *Injury* 2006; 37(Suppl. 3): S25–S32 (Erratum in *Injury* 2007; 38: 1224).
23. Lian JB and Stein GS. Concepts of osteoblast growth and differentiation: basis for modulation of bone cell development and tissue formation. *Crit Rev Oral Biol Med* 1992; 3: 269–305.
24. Langenbach F and Handschel J. Effects of dexamethasone, ascorbic acid and β-glycerophosphate on the osteogenic differentiation of stem cells in vitro. *Stem Cell Res Ther* 2013; 4: 117.
25. Friedenstein AY. Induction of bone tissue by transitional epithelium. *Clin Orthop Relat Res* 1968; 59: 21–37.

26. Ripamonti U. Osteoinduction in porous hydroxyapatite implanted in heterotopic sites of different animal. *Biomaterials* 1996; 17: 31–35.
27. Yamasaki H and Sakai H. Osteogenic response to porous hydroxyapatite ceramics under the skin of dogs. *Biomaterials* 1992; 13: 308–312.
28. Parekh SH, Chatterjee K, Lin-Gibson S, et al. Modulus-driven differentiation of marrow stromal cells in 3D scaffolds that is independent of myosin-based cytoskeletal tensions. *Biomaterials* 2011; 32: 2256–2264.
29. Oh S, Brammer KS, Li YSJ, et al. Stem cell fate dictated solely by altered nanotube dimension. *Proc Natl Acad Sci USA* 2009; 106: 2130–2135.
30. Dalby MJ, Gadegaard N, Tare R, et al. The control of human mesenchymal cell differentiation using nanoscale symmetry and disorder. *Nat Mater* 2007; 6: 997–1003.
31. Langer R and Tirrell DA. Designing materials for biology and medicine. *Nature* 2004; 428: 487–492.
32. Hollister SJ, Maddox RD and Taboas JM. Optimal design and fabrication of scaffolds to mimic tissue properties and satisfy biological constraints. *Biomaterials* 2002; 23: 4095–4103.
33. Miron RJ and Zhang YF. Osteoinduction: a review of old concepts with new standards. *J Dent Res* 2012; 8: 736–744.
34. Maruyama Z, Yoshida CA and Furuichi T. Runx2 determines bone maturity and turnover rate in postnatal bone development and is involved in bone loss in estrogen deficiency. *Dev Dyn* 2007; 236: 1876–1890.
35. Yuan H, Kurashina K, de Bruijn JD, et al. A preliminary study on osteoinduction of two kinds of calcium phosphate ceramics. *Biomaterials* 1999; 20: 1799–1806.
36. Ravindran S, Gao Q, Kotecha M, et al. Biomimetic extracellular matrix-incorporated scaffold induces osteogenic gene expression in human marrow stromal cells. *Tissue Eng Part A* 2012; 18(3–4): 295–309.
37. Wang C, Duan Y, Markovic B, et al. Phenotypic expression of bone-related genes in osteoblasts grown on calcium phosphate ceramics with different phase compositions. *Biomaterials* 2004; 25: 2507–2514.
38. Vogel C, Abreu Rde S, Ko D, et al. Sequence signatures and mRNA concentration can explain two-thirds of protein abundance variation in a human cell line. *Mol Syst Biol* 2010; 6: 400.
39. Mata J, Marguerat S and Bahler J. Post-transcriptional control of gene expression: a genome-wide perspective. *Trends Biochem Sci* 2005; 30: 506–514.
40. Salim A, Nacamuli RP, Morgan EF, et al. Transient changes in oxygen tension inhibits osteogenic differentiation and Runx2 expression in osteoblast. *J Biol Chem* 2004; 279: 40007–40016.
41. Feng G, Jin X, Hu J, et al. Effects of hypoxias and scaffold architecture on rabbit mesenchymal stem cell differentiation towards a nucleus pulposus-like phenotype. *Biomaterials* 2011; 32: 8182–8189.
42. Wang Y, Volloch V, Pindrus MA, et al. Murine osteoblasts regulate mesenchymal stem cells via WNT and cadherin pathways: mechanisms depends on cell–cell behavior. *J Tissue Eng Regen Med* 2007; 1: 39–50.
43. Muller P, Bulnheim U, Diener A, et al. Calcium phosphate surfaces promote osteogenic differentiation of mesenchymal stem cells. *J Cell Mod* 2008; 12: 281–291.
44. Polini A, Pisignano D, Parodi M, et al. Osteoinduction of human mesenchymal stem cells by bioactive composite scaffolds without supplemental osteogenic growth factors. *PLoS One* 2011; 6: e26211.
45. Guha AK, Singh S, Kumaresan R, et al. Mesenchymal cell response to nanosized biphasic calcium phosphate composites. *Colloids Surf B Biointerfaces* 2009; 73: 146–151.
46. Sanchez-Salcedo S, Balas F, Izquierdo-Barba I, et al. In vitro structural changes in porous HA/β-TCP scaffolds in simulated body fluid. *Acta Biomater* 2009; 5: 2738–2751.
47. Jung GY, Park YJ and Han JS. Effects of HA released calcium ion on osteoblasts differentiation. *J Mater Sci Mater Med* 2010; 21: 1649–1654.
48. Zayzafoon M, Fulzele K and McDonald JM. Calmodulin and calmodulin-dependent kinase IIalpha regulate osteoblast differentiation by controlling c-fos expression. *J Biol Chem* 2005; 280: 7049–7059.